LANGMUIR

pubs.acs.org/Langmuir Article

Processing Chitosan for Preparing Chitosan-Functionalized Nanoparticles by Polyelectrolyte Adsorption

Brian K. Wilson and Robert K. Prud'homme*



Cite This: Langmuir 2021, 37, 8517-8524



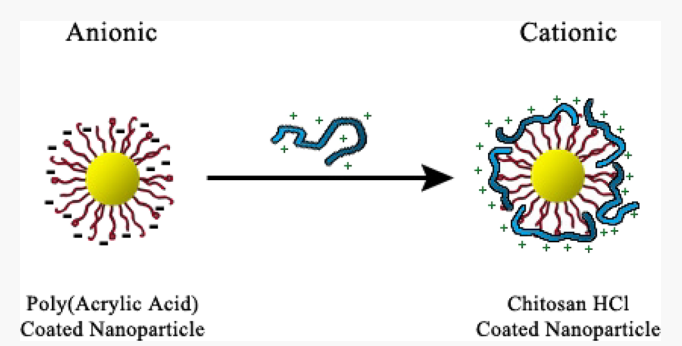
ACCESS

Metrics & More

Article Recommendations

S Supporting Information

ABSTRACT: Chitosan-coated nanoparticles are a promising class of drug delivery vehicles that have been studied as tools for improving the gastrointestinal delivery of therapeutics. Here we present an analysis of chitosan-coated nanoparticles with an emphasis on characterizing the chitosan polymer properties. Cationic nanoparticles are produced by adsorbing a layer of chitosan HCl on an anionic ($-40~\text{mV}~\zeta$ -potential) polyacrylic acid (PAA) coated primary nanoparticle. Commercially available chitosan (90% deacetylated) must be processed into a nearly completely deacetylated HCl salt form (99% deacetylated); otherwise, primary nanoparticle aggregation occurs. Deacetylated chitosan HCl produces stable, cationic ($+35~\text{mV}~\zeta$ -potential)



nanoparticles within 10% of the original anionic particle hydrodynamic diameter at a 1:2 molar ratio of chitosan glucosamine HCl monomers to PAA acrylic acid monomers.

■ INTRODUCTION

Nanoparticles (NPs) and microparticles have received considerable attention as delivery vehicles for both poorly soluble small molecule and biologic active pharmaceutical ingredients (APIs) with an emphasis on engineering the vehicle to increase API solubility, stability, and delivery efficiency. 1 NPs can be designed by using different surface stabilizers, such as ionic surfactants or amphiphilic block copolymers, to impart different surface charges. Nanoparticle surface chemistry and size govern interactions with the mucus layer barriers of the body, which must be overcome in oral delivery applications. A dense layer of neutral polymer such as polyethylene glycol (PEG) is required to minimize mucus adsorption and allow particles to diffuse through mucus,^{3,4} while charged particle surfaces produce mucoadhesive nanoparticles that are tightly bound to the outer surface of mucus layers. 5-7 There are proponents of the strategy that mucodiffusive nanoparticles are the most effective delivery vehicles^{2,8} and proponents of the strategy that mucoadhesion maximizes delivery. 6,9 Much of the earlier work on the effect of nanoparticle surface charge on oral particle delivery has been conducted on polymer latices where the surface polymer is covalently grafted or grown onto the latex surface. 10 This grafting-onto process often does not enable the formation of a dense polymer layer and may leave hydrophobic domains on the latex surface. 11,12

Chitosan has been proposed as a cationic, mucoadhesive material for increased particle adsorption and retention for *in vitro* culture ¹³ and oral, ¹⁴ pulmonary, ⁵ vaginal, ¹⁵ and ocular ¹⁶ delivery. Additional attention has been paid to using chitosan-

coated particles for peptide delivery such as orally dosed insulin and insulin analogs. $^{17-19}$ Chitosan has received particular attention, over other synthetic cationic polymers, since it is biologically sourced and has low toxicity. Commercial grades of chitosan are prepared via hydrolysis of chitin, the N-acetyl form of chitosan, to produce a soluble salt form polymer. This deacetylation reaction must be run to completion or acetylated material must be removed to produce a soluble, low-viscosity product.

Chitosan is anchored onto a NP surface either by covalently grafting onto the particle surface^{20,21} or by electrostatic complexation onto an anionic surface. ^{15–17,22–25} In this work, we electrostatically anchor chitosan onto a negatively charged NP surface where the nanoparticle is formed by the polymer-directed, kinetically controlled precipitation process called Flash NanoPrecipitation (FNP). FNP is a flexible, scalable technique for producing polymeric nanoparticles with a controlled NP size. ^{26,27} Nanoparticles produced by FNP with amphiphilic block copolymers have hydrophobic cores and dense polymer surface coronas. The dense polymer brush on the FNP nanoparticle surface arises from the "bottom up" assembly by diffusion limited aggregation. ¹¹ In this study, we

Received: April 11, 2021 Revised: June 17, 2021 Published: July 8, 2021





produce the initial nanoparticle with a block copolymer having a hydrophobic polystyrene anchoring block and an anionic polyacrylic acid block to create nanoparticles with zeta potentials of -40 mV. A second FNP coating step enables uniform deposition of the cationic chitosan on the NP surface because the rapid micromixing ensures homogeneous mixing of the NPs and chitosan before diffusion limited aggregation and surface adsorption. Polyelectrolyte complexes are well studied both as assemblies on polymer micelles 30,31 and as surface multilayers. The key variable for polyelectrolyte complex formation is the ratio of cationic to anionic charges in the assembly step.

The main focus of this paper is to address the physical chemistry of chitosan polymers that enables electrostatic layerby-layer assembly to produce monodisperse nanoparticles. The outline of the paper is as follows: We show that commercial deacetylated chitosan (90%+ deacetylation) caused nanoparticle aggregation when coated on an anionic nanoparticle. The mechanism of aggregation is shown to be associated with minor amounts of residual acetyl groups. Intrinsic viscosity measurements and zeta potential measurements show that chitosan purification by ethanol solubilization does not alter molecular weight, but neither does it prevent nanoparticle aggregation during coating. Chitosan further deacetylated (99% by NMR) and isolated as the hydrochloride salt enables purely electrostatic anchoring on the nanoparticle surface without hydrophobic nanoparticle bridging or aggregation. The purified chitosan now enables processing of 100-150 nm anionic NPs into cationic +35 mV zeta potential NPs via coating with chitosan. Stable particles are produced when the molar ratio of chitosan HCl monomers to PAA polymer monomers was above 0.5.

EXPERIMENTAL SECTION

Materials. Chitosan (listed as 90%+ deacetylated) was purchased from Spectrum Chemicals (New Brunswick, NJ) and further processed as described below. Polystyrene homopolymer (PS, molecular weight 1.8 kDa) and polystyrene-block-polyacrylic acid (PS-b-PAA, molecular weight 2.3 kDa-b-9.5 kDa) were purchased from Polymer Source, Inc. (Montreal, Canada) and used as is. Hydrochloric acid, acetic acid, sodium acetate, tetrahydrofuran (THF), and sodium chloride were purchased from ThermoFisher Scientific (Waltham, MA). One hundred kiloDalton cutoff PES tangential flow filtration microKros membranes and 6–8 kDa MW cutoff RC-1 dialysis tubing were purchased from Repligen (previously Spectrum Labs, Waltham, MA).

Preparation of Polyacrylic Acid Coated Nanoparticles. Initial anionic nanoparticles are prepared using Flash NanoPrecipitation in a confined impinging jet mixer as previously described. ³³ Five milliliters of THF solution of polystyrene (10 mg/mL) and PS-b-PAA (10 mg/mL) polymers was mixed against 5 mL of deionized MilliQ-grade water with an additional 40 mL of deionized water in the collection bath. The product nanoparticle dispersion was dialyzed against MilliQ-grade water for 24 h with six changes of the 4 L external media. A 1M acetic acid/sodium acetate buffer was added to the dialyzed dispersion to produce a final 15 mM sodium acetate buffer solution with a pH of 5.5.

Processing Chitosan Powder in Fractionated, Hydrochloride Salt. Commercially obtained chitosan was converted into the hydrochloride salt form and fractionated by ethanol precipitation. Five grams of chitosan was added to 60 mL of 200 mM HCl and heated to 80 °C with magnetic stirring for 1 h. This acidic solution was precipitated in 240 mL of room-temperature ethanol, and the chitosan HCl precipitate was isolated by centrifugation. Two additional ethanol precipitations (precipitated product dissolved in 40 mL of water and precipitated into 240 mL of ethanol) were performed to

remove residual HCl and acetylated material. The final precipitated polymer was collected and dissolved in 40 mL of deionized water and lyophilized at $-20~^{\circ}$ C and 150 mTorr for 24 h (VirTis Advantage EL shelf lyophilizer, Warminster, PA) to yield a straw-colored chitosan HCl powder (recovery 4.9 g, 80% yield). Ethanol supernatants were collected and evaporated to recover the ethanol-soluble fraction. The process and structures for the chitosan processing are shown in Figure 1.

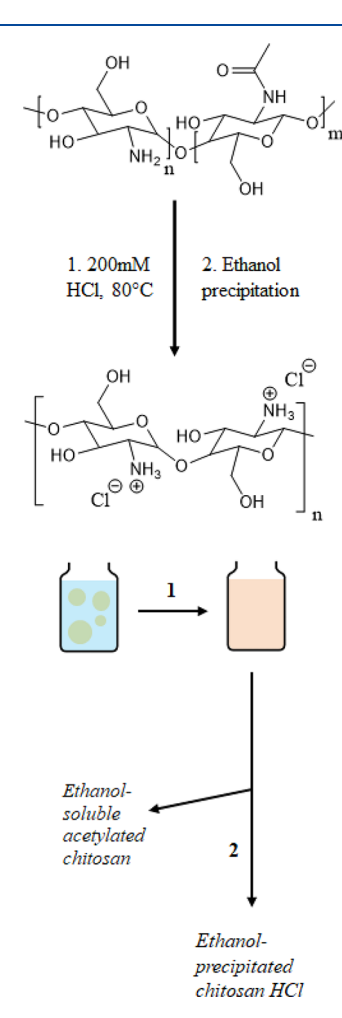


Figure 1. Chitosan HCl processing scheme, with incubation in hydrochloric acid followed by ethanol precipitation from water.

Chitosan materials were analyzed by ¹H NMR and solution viscometry to determine the degree of acetylation and polymer intrinsic viscosity. ¹H NMR spectra were measured in deuterium oxide on a Bruker Avance III 500 MHz spectrometer (Bruker Corporation, Billerica, MA). Polymer solution viscosities were measured in a 250 mM acetic acid, 250 mM sodium acetate buffer on an MCR 501 rheometer using a double gap Couette cell measuring geometry at 100 s⁻¹ applied shear rate (Anton Paar, Graz, Austria).

Coating PAA Nanoparticles with Chitosan. PAA-stabilized nanoparticles were diluted to 0.25 mg/mL in a pH 5.5, 15 mM sodium acetate buffer. This aqueous dispersion was mixed against an aqueous solution of chitosan HCl in a confined impinging jet mixer, with various concentrations of chitosan HCl used to titrate the required chitosan amount to produce a stable, cationic particle surface. Chitosan solutions were prepared by dissolving the polymer powder in MilliQ water followed by 20 min of sonication to fully dissolve the powder. Raw material chitosan was dissolved with a stoichiometric quantity of HCl (equivalent to the moles of glucosamine monomer) from a 1 M stock solution of HCl.

Chitosan Coating Stability Analysis. The stability of the chitosan coating was evaluated by incubating particles coated with 0.5× molar ratio of chitosan HCl to surface PAA in either MilliQ water or 150 mM NaCl for 72 h. The incubated particles were then processed by diafiltration using a hand-driven tangential flow filtration module (100 kDa cutoff, mPES membrane). Incubated dispersions were concentrated approximately five times by volume on the TFF module. Concentrated dispersions were rediluted to the original volume with a pH 5.5, 10 mM acetate buffer with 5 mM NaCl. The buffer-exchanged dispersions were concentrated five times and diluted in measurement buffer for another four cycles to remove incubation salts and unbound chitosan.

Particle Characterization by DLS and *ζ*-Potential Measurement. Nanoparticle hydrodynamic diameter, polydispersity, and *ζ*-potential were measured using a ZetaSizer ZS (Malvern Instruments, Malvern, UK). All measurements were performed in a pH 5.5, 10 mM sodium acetate buffer with 5 mM NaCl in automatic mode at 25 °C. Samples containing existing salt buffers are diluted to match the standard measurement buffer conditions. Data are presented as an average of triplicate measurements.

■ RESULTS AND DISCUSSION

Commercial (90%+) Deacetylated Chitosan Processing and Characterization. Figure 2 shows the particle size

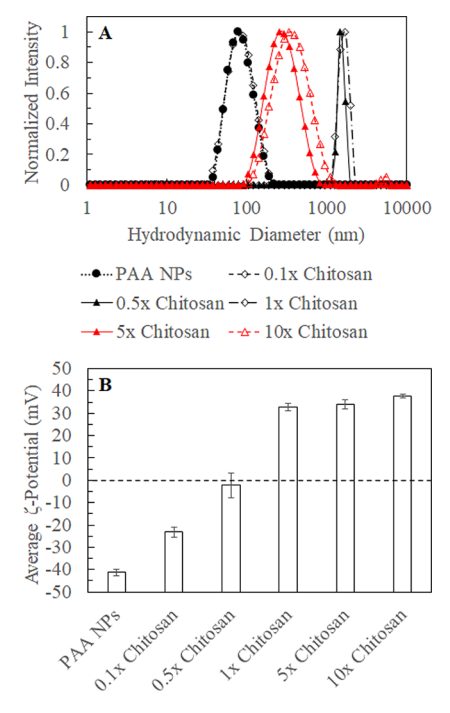


Figure 2. Raw chitosan material fails to produce well-dispersed coated nanoparticles. (A) Particle size distribution for each of the indicated formulations. The equivalent numbers (e.g., 0.1×) indicate the molar ratio of chitosan polymer to PAA-stabilized nanoparticles. (B) ζ-Potential measurement of the same particles. Error bars are \pm standard deviation of triplicate measurements.

distributions and zeta potential measurements for the base PAA anionic nanoparticles (100–125 nm) and particles coated with the commercial chitosan. When using the unprocessed raw chitosan material, the cationic particles produced are aggregates of the primary anionic particles. Solutions of the raw material chitosan are slow-dissolving and require extensive sonication to reduce their turbidity, implying that there is a poorly soluble fraction of chitosan in the raw material.

Purification and Analysis of the Chitosan HCl Material. The failure of the raw chitosan material to form well-dispersed cationic particles motivated the development of a method for processing the chitosan into the hydrochloride salt followed by fractionation to remove residual hydrophobic acetylated material. ¹H NMR analysis of the processed material and ethanol-soluble fraction is shown in Figure 3. The degree

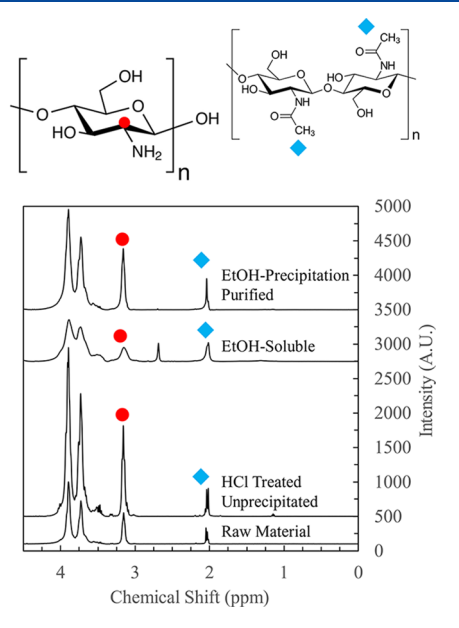


Figure 3. Chitosan ¹H NMR characterization. The degree of deacetylation is calculated from the ratio of the 2.05 ppm peak (methyl of chitin) and the 3.15 ppm peak (amine-adjacent ring proton of glucosamine).

of acetylation is calculated from the ratio of the indicated protons and is listed in Table 1. The raw material has a 91.2%

Table 1. Chitosan Polymer Properties

material	deacetylation (%)	$[\eta]$ (mL/mg)	$k_{ m H}$	average MW _V (kDa)
HCl- treated raw material	94.0 ± 0.9	0.0372 ± 0.0011	2.08 ± 0.12	19.9
ethanol- soluble fraction	89.7 ± 1.3	0.0317 ± 0.0019	4.74 ± 0.57	16.3
purified product	99.9 ± 0.8	0.0689 ± 0.0006	0.67 ± 0.012	43.5
raw material	91.2 ± .2			

degree of deacetylation (rising to 94.0% after HCl treatment), the ethanol-soluble fraction of the commercial starting material has an 89.7% degree of deacetylation, and the purified ethanol-precipitated material has a 99.9% degree of deacetylation.

Polymer viscosities were measured in an acetate buffer as shown in Figure 4 for the unfractionated HCl-treated material, the ethanol-soluble material, and the ethanol-precipitated purified polymer. The plot of viscosity versus concentration was converted into a Huggins plot of specific viscosity divided by concentration versus concentration as also shown in Figure 4. Extrapolation of this plot to zero concentration yields the intrinsic viscosity of the polymer. The purified chitosan

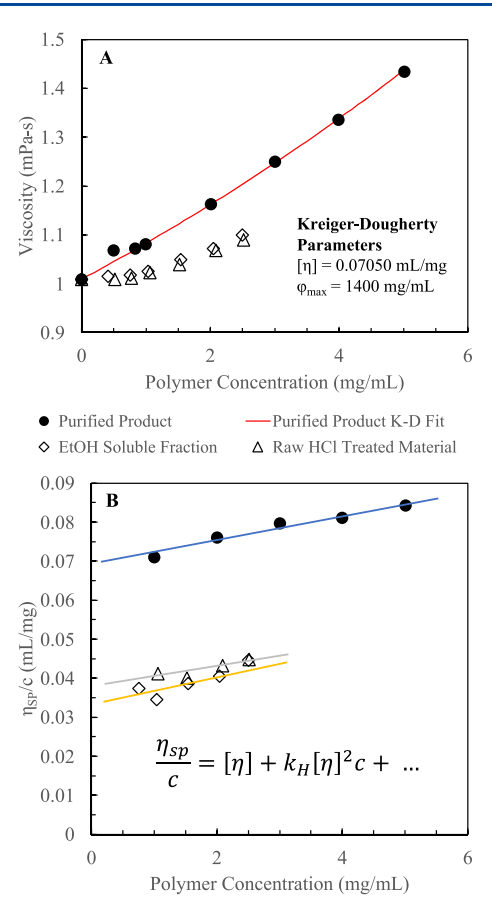


Figure 4. Chitosan viscometry characterization. Chitosan HCl is dissolved in 0.25 M acetic acid/0.25 M sodium acetate buffer for all measurements. (A) Solution viscosities measured for three characterized materials. The Kreiger–Dougherty fit is indicated for the ethanol precipitation purified product with an intrinsic viscosity of 0.071 mL/mg. (B) Huggins plot intrinsic viscosity extrapolation of chitosan polymer intrinsic viscosity.

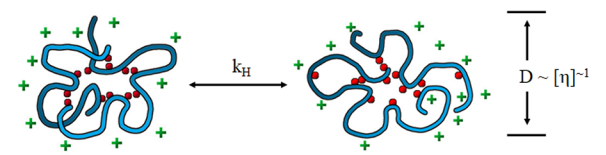
material shows similar intrinsic viscosity calculations from the Huggins plot and the Kreiger–Dougherty fit (0.0689 versus 0.07050 mL/mg). This intrinsic viscosity molecular volume can be correlated to a molecular weight using the known Mark–Houwink parameters for 10-20% acetylated chitosan: $K=1.57\times10^{-4}$ and $a=0.79.^{34}$ The viscosity-averaged molecular weight of the chitosan HCl is 43.5 kDa, while the raw material yields a chitosan MW of 19.9 kDa and the ethanol-soluble fraction yields a chitosan MW of 16.3 kDa, reflective of the collapsed acetylated globule size in the acetate measurement buffer.

As shown in Figure 2, if the initial 90% deacetylated chitosan is used in the coating step at very low chitosan concentrations (0.1 charge equivalents cationic charge to anionic acrylic acid charge), the NP size is not altered, but the NP zeta potential increases from -40 to -20 mV. Some cationic chitosan is adsorbed on the anionic NP surface; however, the strong overall negative charge results in stable NPs. However, at charge ratios of 0.5 and 1.0, flocculation of the NPs is observed. This is consistent with a "charge patch" mechanism of flocculation, wherein the NP surface has patches of cationic chitosan and anionic PAA that enable internanoparticle attractions, bridging, and aggregation. At high charge ratios (5× and 10×), the NPs become fully cationic with a zeta potential of 30 mV. Prior studies of polyelectrolyte multilayer

systems, both on flat surfaces and on coating nanoparticles, have demonstrated equivalent charge reversal of anionic surfaces. ^{24,25} The more interesting observation is that, under these conditions, the NPs aggregate to 300–600 nm sizes. This aggregation of highly charged NPs is not driven by electrostatics but rather by hydrophobic interactions between the acetyl groups on the chitosan. Hydrophobically modified polymers associating on colloid/NP surfaces and causing aggregation of these systems have been widely studied in the context of associating polymers and latex paints and coatings. ^{36–38} Only a few percent of hydrophobic associating sites on a polymer chain can cause bridging between colloids. Hydrophobic associating polymer sites can flip between being anchored on the single NP surface and bridging between two NPs.

The role of these few hydrophobic sites is seen on the chitosan viscosity measurements and when compared to the results on the fully deacetylated chitosan to be discussed below. Analysis of the chitosan materials by ¹H NMR shows that the initial commercial chitosan contains ~10 mol % (based on monomer saccharide) acetyl groups. The intrinsic viscometry results in Figure 4 show the effect of this low level of associative sites, and this is schematically shown in Figure 5.

A. 90% Deacetylated (Commercial Grade)



B. 99% Deacetylated (Purified Material)

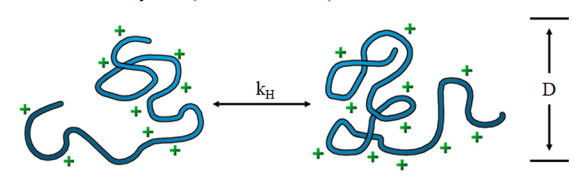


Figure 5. Huggins coefficient $(k_{\rm H})$ impact on polymer coil conformations in solution both for partially acetylated (A) material and for purified nearly completely deacetylated material (B).

The initial chitosan and the alcohol soluble fraction have intrinsic viscosities of $[\eta] \sim 0.03$ mL/mg. Once the chitosan is further deacetylated, the intrinsic viscosity increases to 0.07 mL/mg. The increase in molecular volume is a result of the removal of intrachain associations that have collapsed the chain, with a resulting expansion of the molecular coil. This is what is expected from the theory of associating polymers.^{39–} Note that the commercial material is tuned to be water dispersible at 90%+ deacetylation. Lower levels would result in the insolubility of the polymer in aqueous solution. This phase separation is predicted by the theories of associating polymers, where chain collapse is followed by precipitation and phase separation at higher hydrophobic substitution levels. 39,41,42 The acid treatment does not cause covalent cleavage of the glucosamine sugar backbone, which would result in a decrease in intrinsic viscosity, but removes essentially all hydrophobic associating sites and enables expansion of the chain.

The Huggins coefficient determined from the slope of the data in the specific viscosity versus concentration shows the effect of *intermolecular* interactions between chitosan chains. As

shown in the schematic in Figure 5, the Huggins coefficient, the second-order coefficient of the specific viscosity with polymer concentration (Figure 5), indicates the strength of intermolecular interactions. The value for the fully deacetylated chitosan is $k_{\rm H}$ = 0.67, which is characteristic for soluble polymers in good solvent, which is the case for the 0.5 M acetate salt solutions used for the viscosity measurements. For neutral polysaccharides with uniform hydroxypropyl substitution, the Huggins coefficient varies from $k_{\rm H}=0.79$ for the unsubstituted guar to 0.32 for 1.58 molar substitution (i.e., hydroxypropyl groups per sugar residue);44 the decrease indicates a transition from an expanded chain in a good solvent to a chain with weak attractive interactions between chains. In contrast, for polyelectrolyte polymers and colloids, the repulsive interactions dominate. For soluble hydrophobically modified polyelectrolyte polymers, Huggins coefficients greater than 1 are observed $(k_{\rm H}=1.19^{40,45})$, indicating stronger chain repulsions. However, for the commercial chitosan and the alcohol soluble fractions of that polymer, the Huggins coefficients are $k_{\rm H}$ = 2.08 and 4.74, respectively. Values substantially above 1 are only observed for dense polyelectrolyte microgel particles. 46 For acetylated chitosan the hydrophobic sites are organized inside the polymer coil or cluster to form a microgel core, and the cationic amine groups are localized on the surface as shown in Figure 5. This structure presents the cationic charged groups more compactly than they would be if the hydrophobic core was not constraining their location, as for a soluble polymer coil.

Coating PAA-Stabilized Nanoparticles with Purified Chitosan HCl. Figure 6 shows the average hydrodynamic diameter and average ζ -potential of PAA nanoparticles coated

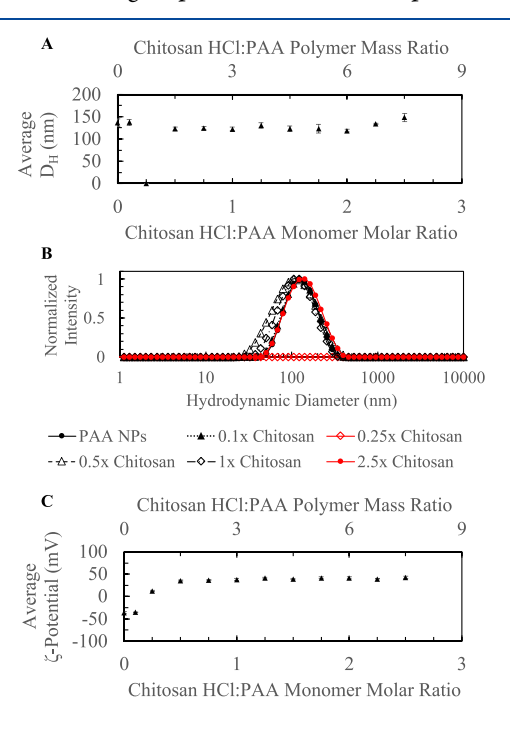


Figure 6. Chitosan-coated PAA nanoparticle average sizes and zeta potentials using purified chitosan HCl product. (A) Average hydrodynamic diameter in nanometers as a function of chitosan HCl/PAA molar and mass ratios. (B) Particle size distribution of several chitosan-coated PAA nanoparticles from panel (A). (C) Average ζ-potentials of same formulations in mV. Error bars are \pm standard deviation of triplicate measurements.

with the purified chitosan HCl polymer. Nanoparticle size cannot be accurately measured by the DLS analysis algorithm used for 0.25 molar equivalents of chitosan as the PAA nanoparticles are aggregated at this condition. Beyond this point, the nanoparticles produced are stable, monodisperse, and cationic. The nanoparticle hydrodynamic diameter remains like the base PAA nanoparticle of \sim 120 nm, but the ζ -potential is reversed. Particle size distributions for several key compositions are also shown in Figure 6 to demonstrate the monodisperse nature of the chitosan-coated nanoparticles. Measurements of unbound chitosan are given in the Supporting Information, with less than 5% of the chitosan present as unbound polymer in solution at the maximum molar ratio of 3:1.

The stability of the chitosan coating over time was evaluated by measuring the zeta potential and hydrodynamic diameter after using tangential flow filtration to exchange the incubation media for DLS measurement buffer. Nanoparticle size distributions and average ζ -potentials are shown in Figure 7.

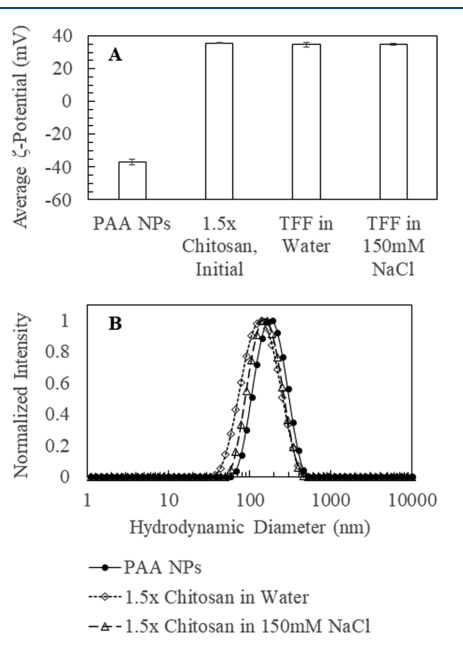


Figure 7. Stability of chitosan HCl coating in both MilliQ water and 150 mM NaCl for 72 h after TFF diafiltration. (A) Average ζ -potential of 0.5× (molar ratio) chitosan-coated nanoparticles. (B) Particle size distributions of initial and coated formulations. Error bars are \pm standard deviation of triplicate measurements.

The chitosan-coated particles retain the same hydrodynamic diameter and cationic ζ -potential, indicating that the adsorbed chitosan remains on the particle surface and confers the same average properties.

The difference in chitosan solution structure between the completely deacetylated form relative to the 90% deacetylated form makes a qualitative difference in the coated NPs that can be produced. There are three regimes of charge equivalence to consider. First, for both chitosans, at low charge equivalents, the overall NP size is not substantially changed by low levels of chitosan adsorption, and the anionic NP zeta potential increases (Figures 2 and 6). The second regime is the aggregation upon charge neutralization. In both systems, when charge neutrality is approached, the NPs flocculate by a charge-patch mechanism. However, the striking difference between the two polymer systems is the range of charge equivalents

where aggregation is observed. The 90%+ deacetylated chitosan produces large aggregates at charge equivalent ratios of 0.5–1.0 because the flocculation is driven by charge-patch interactions and by attractive interactions between hydrophobic acetyl groups on the chitosan (Figure 2). For the completely deacetylated chitosan, the only attractive mechanism is charge-patch bridging, and it is only observed at the ratio of 0.25 (Figure 6). For the fully deacetylated chitosan, the transition from highly cationic to highly anionic happens over a narrow range of composition. These three regimes of coating are depicted in Figure 8.

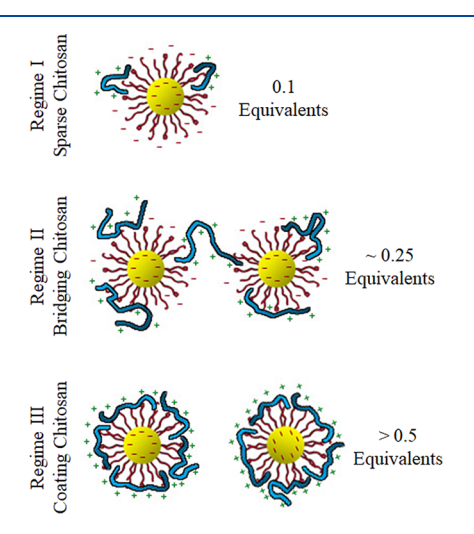


Figure 8. Three regimes of nanoparticle coating with chitosan HCl as feed concentration of chitosan HCl increases. For the deacetylated purified material, the interactions are purely electrostatic, including the regime II bridging, while the commercial acetylated material also has hydrophobic interactions between acetylated domains that drive aggregation of primary anionic nanoparticles, even in the regime III of excess chitosan HCl.

Polyelectrolytes in deionized water typically require a pH far above the monomer nominal pK_a to achieve a highly ionized molecule. The system used here consists of a buffer with an ionic strength in excess of the polyelectrolyte monomers that assists with polymer ionization. Polyelectrolytes in adsorbed bilayers or multilayers show increased ionization. For PAA complexed with poly(allylamine) (PAH, a polyamine comparable to chitosan), the PAA and PAH monomers show over 90% ionization at pH 5.5. The monomer ratio between polyelectrolytes very nearly matches the charge ratio between the two polyelectrolytes.

Both the titration plot in Figure 6 and the coating stability analysis in Figure 7 show that highly cationic NPs are produced at less than 1 charge equivalence between polyelectrolytes. Flash NanoPrecipitation produces particles with a dense polymer surface on the order of 1 polymer chain per square nanometer of surface. In this dense brush configuration, the adsorbing approximately 40 kDa chitosan cannot access the acrylic acid monomers near the surface of the particle hydrophobic core due to both steric repulsion between the polymer chains and adsorption of the polymer on the outermost layer of the PAA stabilizing corona. Stoichiometric titration requirements are determined not only by the number of moles of monomers present but also by the ability of the polymers to interact with and access dense brush regions.

The third regime is the region of high cationic charge ratio. For the unpurified, 90% deacetylated chitosan, high charge ratios ($5 \times$ and $10 \times$) produce NPs with zeta potentials of +32 mV, but the particle size is 600 nm, much larger than the primary anionic NP size of 120 nm. However, the fully acetylated polymer produces 150 nm NPs with +40 mV surfaces for all charge ratios of 0.5 and greater. The uniformity of sizes and charges is a result of the purely electrostatic interactions with the anionic NP surface and the uniform contacting of the chitosan and anionic NP during the rapid micromixing associated with FNP. These chitosan-coated NPs produce extremely stable cationic surfaces that resist polymer displacement by ion exchange against 150 mM salts, resist swelling in DI water, and resist changes in zeta potential after ultrafiltration removal of unbound chitosan. These results are like previously observed systems of quaternized amine polyelectrolyte micelles but with a much smaller instability window (regime II).31

CONCLUSIONS

We have demonstrated the facile production of chitosan-coated cationic nanoparticles using a simple polyelectrolyte layer adsorption process without any required covalent modification of the chitosan to anchor it to a nanoparticle surface. Titrating the amount of coating polymer reveals that only a 1:2 molar ratio of chitosan HCl monomer to PAA monomer is required to form stable, cationic nanoparticles. A substoichiometric quantity of coating polymer implies that the full PAA stabilizer corona is not accessible to the higher-molecular-weight chitosan HCl. Nanoparticles designed for oral delivery of therapeutic-releasing nanoparticles can be easily modified in this manner to change the particle surface charge.

Complete deacetylation of the chitosan is necessary to obtain optimal NP properties. Directly using the as-received material resulted in aggregated nanoparticles with substantially larger hydrodynamic diameters. Since parenteral administration requires NP sizes less than 400 nm to enable circulation, the NPs produced by the as-received chitosan would not be usable, but the 99% deacetylated chitosan does enable the production of stable, monodisperse cationic particles by coating an anionic primary nanoparticle. When using biopolymers as nanoparticle materials, analyzing the polymer composition and properties is critical for understanding the physical state and suitability of the biopolymer for the intended nanoparticle application. The FNP process using preformed anionic NPs and fully deacetylated chitosan as the two inlet flow streams provides a robust platform to produce these cationic NPs.

ASSOCIATED CONTENT

3 Supporting Information

The Supporting Information is available free of charge at https://pubs.acs.org/doi/10.1021/acs.langmuir.1c00990.

Analysis of chitosan adsorption efficiency using a fluorescently tagged chitosan (PDF)

AUTHOR INFORMATION

Corresponding Author

Robert K. Prud'homme — Department of Chemical and Biological Engineering, Princeton University, Princeton, New Jersey 08544, United States; orcid.org/0000-0003-2858-

0097; Phone: 609-258-4577; Email: prudhomm@princeton.edu; Fax: 609-258-0211

Author

Brian K. Wilson – Department of Chemical and Biological Engineering, Princeton University, Princeton, New Jersey 08544, United States

Complete contact information is available at: https://pubs.acs.org/10.1021/acs.langmuir.1c00990

Notes

The authors declare no competing financial interest.

ACKNOWLEDGMENTS

This work was supported by the National Science Foundation Graduate Research Fellowship under Grant DGA 1148900. The authors acknowledge the use of Princeton's Imaging and Analysis Center, which is partially supported through the Princeton Center for Complex Materials (PCCM), a National Science Foundation (NSF)-MRSEC program (DMR-2011750).

■ REFERENCES

- (1) Desai, P. P.; Date, A. A.; Patravale, V. B. Overcoming Poor Oral Bioavailability Using Nanoparticle Formulations Opportunities and Limitations. *Drug Discov. Today Technol.* **2012**, *9*, e87–e95.
- (2) Date, A. A.; Hanes, J.; Ensign, L. M. Nanoparticles for Oral Delivery: Design, Evaluation and State-of-the-Art. *J. Controlled Release* **2016**, 240, 504–526.
- (3) Maisel, K.; Reddy, M.; Xu, Q.; Chattopadhyay, S.; Cone, R.; Ensign, L. M.; Hanes, J. Nanoparticles Coated with High Molecular Weight PEG Penetrate Mucus and Provide Uniform Vaginal and Colorectal Distribution in Vivo. *Nanomedicine* **2016**, *11*, 1337–1343.
- (4) Lu, H. D.; Spiegel, A. C.; Hurley, A.; Perez, L. J.; Maisel, K.; Ensign, L. M.; Hanes, J.; Bassler, B. L.; Semmelhack, M. F.; Prud'homme, R. K. Modulating Vibrio Cholerae Quorum-Sensing-Controlled Communication Using Autoinducer-Loaded Nanoparticles. *Nano Lett.* **2015**, *15*, 2235–2241.
- (5) Yamamoto, H.; Kuno, Y.; Sugimoto, S.; Takeuchi, H.; Kawashima, Y. Surface-Modified PLGA Nanosphere with Chitosan Improved Pulmonary Delivery of Calcitonin by Mucoadhesion and Opening of the Intercellular Tight Junctions. *J. Controlled Release* **2005**, *102*, 373–381.
- (6) Banerjee, A.; Lee, J.; Mitragotri, S. Intestinal Mucoadhesive Devices for Oral Delivery of Insulin. *Bioeng. Transl. Med.* **2016**, *1*, 338–346.
- (7) Roger, E.; Lagarce, F.; Garcion, E.; Benoit, J.-P. Biopharmaceutical Parameters to Consider in Order to Alter the Fate of Nanocarriers after Oral Delivery. *Nanomedicine* **2010**, *5*, 287–306.
- (8) Lai, S. K.; Wang, Y. Y.; Hanes, J. Mucus-Penetrating Nanoparticles for Drug and Gene Delivery to Mucosal Tissues. *Adv. Drug Delivery Rev.* **2009**, *61*, 158–171.
- (9) Serra, L.; Doménech, J.; Peppas, N. A. Engineering Design and Molecular Dynamics of Mucoadhesive Drug Delivery Systems as Targeting Agents. Eur. J. Pharm. Biopharm. 2009, 71, 519–528.
- (10) Ballauff, M. Spherical Polyelectrolyte Brushes. *Prog. Polym. Sci.* **2007**, 32, 1135–1151.
- (11) Pagels, R. F.; Edelstein, J.; Tang, C.; Prud'homme, R. K. Controlling and Predicting Nanoparticle Formation by Block Copolymer Directed Rapid Precipitations. *Nano Lett.* **2018**, *18*, 1139–1144.
- (12) Michalek, L.; Barner, L.; Barner-Kowollik, C. Polymer on Top: Current Limits and Future Perspectives of Quantitatively Evaluating Surface Grafting. *Adv. Mater.* **2018**, *30*, 1706321.
- (13) Chronopoulou, L.; Massimi, M.; Giardi, M. F.; Cametti, C.; Devirgiliis, L. C.; Dentini, M.; Palocci, C. Chitosan-Coated PLGA

- Nanoparticles: A Sustained Drug Release Strategy for Cell Cultures. *Colloids Surf., B* **2013**, *103*, 310–317.
- (14) Mazzarino, L.; Travelet, C.; Ortega-Murillo, S.; Otsuka, I.; Pignot-Paintrand, I.; Lemos-Senna, E.; Borsali, R. Elaboration of Chitosan-Coated Nanoparticles Loaded with Curcumin for Mucoadhesive Applications. J. Colloid Interface Sci. 2012, 370, 58–66.
- (15) Jøraholmen, M. W.; Vanić, Ž.; Tho, I.; Škalko-Basnet, N. Chitosan-Coated Liposomes for Topical Vaginal Therapy: Assuring Localized Drug Effect. *Int. J. Pharm.* **2014**, *472*, 94–101.
- (16) Abdelbary, G. Ocular Ciprofloxacin Hydrochloride Mucoadhesive Chitosan-Coated Liposomes. *Pharm. Dev. Technol.* **2011**, *16*, 44–56
- (17) Takeuchi, H.; Matsui, Y.; Sugihara, H.; Yamamoto, H.; Kawashima, Y. Effectiveness of Submicron-Sized, Chitosan-Coated Liposomes in Oral Administration of Peptide Drugs. *Int. J. Pharm.* **2005**, 303, 160–170.
- (18) Guo, J.; Ping, Q.; Jiang, G.; Huang, L.; Tong, Y. Chitosan-Coated Liposomes: Characterization and Interaction with Leuprolide. *Int. J. Pharm.* **2003**, *260*, 167–173.
- (19) Fonte, P.; Nogueira, T.; Gehm, C.; Ferreira, D.; Sarmento, B. Chitosan-Coated Solid Lipid Nanoparticles Enhance the Oral Absorption of Insulin. *Drug Deliv. Transl. Res.* **2011**, *1*, 299–308.
- (20) Popat, A.; Liu, J.; Lu, G. Q. M.; Qiao, S. Z. A PH-Responsive Drug Delivery System Based on Chitosan Coated Mesoporous Silica Nanoparticles. *J. Mater. Chem.* **2012**, *22*, 11173–11178.
- (21) Guo, L.; Yan, D. D.; Yang, D.; Li, Y.; Wang, X.; Zalewski, O.; Yan, B.; Lu, W. Combinatorial Photothermal and Immuno Cancer Therapy Using Chitosan-Coated Hollow Copper Sulfide Nanoparticles. ACS Nano 2014, 8, 5670–5681.
- (22) Takeuchi, H.; Yamamoto, H.; Niwa, T.; Hino, T.; Kawashima, Y. Enteral Absorption of Insulin in Rats from Mucoadhesive Chitosan-Coated Liposomes. *Pharm. Res.* **1996**, *13*, 896–901.
- (23) Dreaden, E. C.; Kong, Y. W.; Morton, S. W.; Correa, S.; Choi, K. Y.; Shopsowitz, K. E.; Renggli, K.; Drapkin, R.; Yaffe, M. B.; Hammond, P. T. Tumor-Targeted Synergistic Blockade of MAPK and PI3K from a Layer-by-Layer Nanoparticle. *Clin. Cancer Res.* **2015**, *21*, 4410–4419.
- (24) Vázquez, E.; Dewitt, D. M.; Hammond, P. T.; Lynn, D. M. Construction of Hydrolytically-Degradable Thin Films via Layer-by-Layer Deposition of Degradable Polyelectrolytes. *J. Am. Chem. Soc.* **2002**, *124*, 13992–13993.
- (25) Gu, L.; Deng, Z. J.; Roy, S.; Hammond, P. T. A Combination RNAi-Chemotherapy Layer-by-Layer Nanoparticle for Systemic Targeting of KRAS/P 53 with Cisplatin to Treat Non–Small Cell Lung Cancer. Clin. Cancer Res. 2017, 23, 7312–7323.
- (26) Johnson, B. K.; Prud'homme, R. K. Flash NanoPrecipitation of Organic Actives and Block Copolymers Using a Confined Impinging Jets Mixer. *Aust. J. Chem.* **2003**, *56*, 1021–1024.
- (27) Zhu, Z.; Margulis-Goshen, K.; Magdassi, S.; Talmon, Y.; Macosko, C. W. Polyelectrolyte Stabilized Drug Nanoparticles via Flash Nanoprecipitation: A Model Study with β -Carotene. *J. Pharm. Sci.* **2010**, 99, 4295–4306.
- (28) Johnson, B. K.; Prud'homme, R. K. Mechanism for Rapid Self-Assembly of Block Copolymer Nanoparticles. *Phys. Rev. Lett.* **2003**, *91*, 118302.
- (29) Johnson, B. K.; Prud'homme, R. K. Chemical Processing and Micromixing in Confined Impinging Jets. *AIChE J.* **2003**, *49*, 2264–2282.
- (30) Pergushov, D. V.; Müller, A. H. E.; Schacher, F. H. Micellar Interpolyelectrolyte Complexes. *Chem. Soc. Rev.* **2012**, *41*, 6888–6901
- (31) Lysenko, E. A.; Chelushkin, P. S.; Bronich, T. K.; Eisenberg, A.; Kabanov, V. A.; Kabanov, A. V. Formation of Multilayer Polyelectrolyte Complexes by Using Block Ionomer Micelles as Nucleating Particles. *J. Phys. Chem. B* **2004**, *108*, 12352–12359.
- (32) Choi, J.; Rubner, M. F. Influence of the Degree of Ionization on Weak Polyelectrolyte Multilayer Assembly. *Macromolecules* **2005**, *38*, 116–124.

- (33) Markwalter, C. E.; Pagels, R. F.; Wilson, B. K.; Ristroph, K. D.; Prud'homme, R. K. Flash Nanoprecipitation for the Encapsulation of Hydrophobic and Hydrophilic Compounds in Polymeric Nanoparticles. *J. Visualized Exp.* **2019**, 2019, No. e58757.
- (34) Kasaai, M. R.; Arul, J.; Charlet, G. Intrinsic Viscosity—Molecular Weight Relationship for Chitosan. *J. Polym. Sci. Part B Polym. Phys.* **2000**, 38, 2591–2598.
- (35) Halverson, F.; Panzer, H. Flocculating Agents, Encyclopedia of Chemical Technology, Volume 10; Wiley, New York, 1980.
- (36) Santore, M. M.; Russel, W. B.; Prud'homme, R. K. Influence of Associating Polymer on the Physical Properties of Dispersions. In Polymeric Materials Science and Engineering, Proceedings of the ACS Division of Polymeric Materials Science and Engineering; 1989; Vol. 61, pp. 539–543.
- (37) Santore, M. M.; Russel, W. B.; Prud'homme, R. K. A Two-Component Model for the Phase Behavior of Dispersions Containing Associative Polymer. *Macromolecules* **1989**, 22, 1317–1325.
- (38) Karlson, L.; Joabsson, F.; Thuresson, K. Phase Behavior and Rheology in Water and in Model Paint Formulations Thickened with HM-EHEC: Influence of the Chemical Structure and the Distribution of Hydrophobic Tails. *Carbohydr. Polym.* **2000**, *41*, 25–35.
- (39) Cates, M. E.; Witten, T. A. Chain Conformation and Solubility of Associating Polymers. *Macromolecules* **1986**, *19*, 732–739.
- (40) English, R. J.; Gulati, H. S.; Jenkins, R. D.; Khan, S. A. Solution Rheology of a Hydrophobically Modified Alkali-Soluble Associative Polymer. J. Rheol. 1997, 41, 427–444.
- (41) Rubinstein, M.; Dobrynin, A. V. Solutions of Associative Polymers. *Trends Polym. Sci.* **1997**, *5*, 181–186.
- (42) Sing, C. E.; Alexander-Katz, A. Equilibrium Structure and Dynamics of Self-Associating Single Polymers. *Macromolecules* **2011**, 44, 6962–6971.
- (43) Winnik, M. A.; Yekta, A. Associative Polymers in Aqueous Solution. Curr. Opin. Colloid Interface Sci. 1997, 2, 424–436.
- (44) Cheng, Y.; Brown, K. M.; Prud'homme, R. K. Characterization and Intermolecular Interactions of Hydroxypropyl Guar Solutions. *Biomacromolecules* **2002**, *3*, 456–461.
- (45) Ng, W. K.; Tam, K. C.; Jenkins, R. D. Evaluation of Intrinsic Viscosity Measurements of Hydrophobically Modified Polyelectrolyte Solutions. *Eur. Polym. J.* **1999**, *35*, 1245–1252.
- (46) Goring, D. A. I.; Rezanowich, A. The Huggins Viscosity Coefficient for a Polyelectrolyte Microgel. *J. Colloid Sci.* **1960**, *15*, 472–482.
- (47) Swift, T.; Swanson, L.; Geoghegan, M.; Rimmer, S. The PH-Responsive Behaviour of Poly(Acrylic Acid) in Aqueous Solution Is Dependent on Molar Mass. *Soft Matter* **2016**, *12*, 2542–2549.
- (48) Ferrand-Drake del Castillo, G.; Hailes, R. L. N.; Dahlin, A. Large Changes in Protonation of Weak Polyelectrolyte Brushes with Salt Concentration—Implications for Protein Immobilization. *J. Phys. Chem. Lett.* **2020**, *11*, 5212–5218.